J. CHEM. SOC. FARADAY TRANS., 1992, 88(18), 2565–2574

FARADAY RESEARCH ARTICLE

Interferences in Molecular Photofragmentation and their Effect on Vector Properties

Laurens D. A. Siebbeles and J. Alberto Beswick
LURE, Université de Paris Sud, Orsay, France

Selected examples are presented to demonstrate the effects in molecular photofragmentation processes of quantum interferences due to simultaneous transitions from one initial state to several dissociative pathways giving the same final fragments. Particular emphasis is given to the effect on vector properties such as the ejection anisotropy, the alignment and orientation of photofragments, and the fluorescence polarization. In many cases these interference effects are extremely sensitive to details of the potential-energy surfaces and inter-electronic couplings in excited states.

1. Introduction

Molecular photodissociation studies are motivated by fundamental reasons as well as by their importance in the fields of atmospheric chemistry and astrophysics. From the fundamental viewpoint, molecular fragmentation induced by the absorption of light constitutes one of the most basic processes in photochemistry. Detailed knowledge of the excitation from an initial parent state and the evolution into separated fragments *via* a 'half-collision', is needed in order to understand fully the dynamics of photodissociation processes.[1] Also, laser control of photochemical reactions is an important goal in the field of photochemistry. Ideally one would like to drive particular experimental outcomes, such as selected radicals in well defined final states, by monitoring the laser frequency, intensity, pulse shape or its polarization.

The field of photofragmentation has undergone notable experimental progress due to the development of supersonic beams in conjunction with diverse laser techniques, which allow not only excitation of a parent molecule to a well defined state but also detection of photofragments with very high efficiency.[2] Laser-induced fluorescence is currently used to obtain complete vibrational and rotational populations, as well as orientational information on the photofragments.[3] Time-of-flight spectrometers are used to obtain high-resolution angular and translational energy distributions.[4] An alternative technique uses narrow-bandwidth tunable lasers to interrogate Doppler profiles. This latter technique not only provides translational energy distributions but also vector correlations between translational and rotational motion of photofragments.[5] Femtosecond lasers are used to study real-time dynamics in the earlier stages of the fragmentation.[6] Supersonic nozzle beams can prepare cooled molecular species with well characterized initial states and can produce van der Waals complexes and clusters for dissociation studies.[7] One important application of this technique uses the van der Waals molecules formed in a jet as precursors for studying oriented bimolecular reactions induced by photon absorption.[8] Infrared and visible lasers are used to deposit energy into specific molecular vibrations to enable the study of photofragmentation dynamics of vibrationally excited molecules (vibrationally mediated photodissociation), and also to excite high overtones from which the molecules undergo unimolecular decomposition.[9] The molecules are usually randomly oriented in the initial state, but experiments can now also be conducted on oriented molecules in molecular beams.[10]

When considering a general photodissociation process in an isolated molecule,

$$\text{molecule} + \text{light} \rightarrow \text{fragments}$$

the first obvious questions concern the number and the nature of the fragments. A more detailed knowledge of the process would require determination of:

(i) the final states of the fragments associated with internal degrees of freedom (electronic, vibrational and rotational) as well as the translational motion (relative kinetic energies and angular distribution of the photofragments). (ii) The correlations between the motion of the fragments. (iii) The total photodissociation probability (cross-section) and the branching ratio between fragmentation and fluorescence. (iv) The timescale for the overall process and possible timescale separation. This can be obtained directly through real-time experiments using pulsed pump and probe lasers, or in some favourable cases from linewidth measurements in c.w. energy-resolved experiments. (v) The dependence on frequency, polarization, and intensity of the incident light as well as on the pulse duration in the case of time-dependent experiments. (vi) The influence of the initial state of the molecule (selected rovibrational initial states, initially oriented molecules).

From the theoretical point of view, the questions raised are intimately connected to the results of the above measurements. Some of these questions are: (i) What are the mechanisms for dissociation? (ii) How does the molecule evolve in time when excited with a pulsed laser? (iii) What are the effects of the initial conditions of the molecule and the excitation conditions? (iv) How is the excess energy redistributed among the various degrees of freedom of the system? (v) To what particular parameters of the problem are the different observables most sensitive?

Loosely speaking, the mechanisms for photodissociation can be classified as direct (prompt) dissociation or as predissociation (delayed).[1,11,12] Direct dissociation is characterized by broad structureless absorption spectra with typical linewidths of the order of 10000 cm^{-1}. This corresponds to dissociation lifetimes of the order of 10^{-14}–10^{-15} s, *i.e.* of the order of a vibrational period. In the simplest case direct dissociation occurs by excitation above the exit barriers of a bond reaction coordinate. Just below the barrier, dissociation can still occur by tunnelling and this results in delayed fragmentation. Hydrogen-containing molecules provide examples of this tunnelling predissociation, the barrier being due to centrifugal energy (predissociation by rotation).[12]

It is, however, also possible to observe delayed dissociation when excitation takes place to bound levels of an excited state which are weakly coupled to the dissociative continuum of another state. The states can be associated with different adiabatic electronic configurations in which case the coupling is provided by non-adiabatic couplings (electronic predissociation),[12] or, if derived from the same electronic configuration, coupled by intrastate vibrational interactions (vibrational predissociation).[13] In these two cases, the excited-state lifetime is longer than a vibrational period and in some cases even longer than a rotational period (slow predissociation). The absorption spectra will then be characterized by some sort of vibrational or rotational resolution as opposed to the structureless bell-shaped spectra observed in the case of direct dissociation. Also, the long lifetimes of the excited state will enhance the probability of excited-state energy redistribution and allow the excited molecule to rotate before it dissociates. Therefore the angular distributions and the final-state populations of the photofragments are very different from those observed in direct dissociation.

Two complementary theoretical descriptions of photofragmentation dynamics can be provided involving energy-resolved[14] variables such as cross-sections and quantum yields, and time-resolved variables, which specify the time evolution of the dissociative state.[15] Note at this point that dissociation can be described formally as one half of a collision between the same fragments.[1] In this context, predissociation can be viewed as collision complexes (resonances), tunnelling predissociation corresponding to shape resonances and electronic or vibrational predissociation corresponding to Feshbach resonances.

From the general theoretical point of view, the photodissociation observables can be classified into two categories: (i) scalar quantities, *e.g.* cross-sections for absorption, for resonance fluorescence, for Raman scattering, for photodissociation and population probabilities for the different exit channels. (ii) Vectorial quantities, *e.g.* angular correlations, fragment polarization and angular momentum correlations.

In recent years there has been an increasing interest in the measurement of vector properties of photofragments as a means to obtaining additional information on the dynamics of molecular interactions in excited states.[16] The most obvious property is the angular distribution of photofragments in space. Even for initially randomly oriented molecules this distribution is in general anisotropic.[18–20] The incident light introduces (by its polarization or its direction of propagation) a privileged axis in space. Since there is a $|\boldsymbol{\mu}\cdot\boldsymbol{e}|^2$ dependence of the photon absorption probability ($\boldsymbol{e}$ being the polarization vector and $\boldsymbol{\mu}$ the electric dipole moment) light will preferentially excite molecules with $\boldsymbol{e}$ parallel to $\boldsymbol{\mu}$. Now $\boldsymbol{\mu}$ has a well defined orientation with respect to the internuclear axis $\boldsymbol{R}$ and in rapid dissociation $\boldsymbol{v}$ (the relative velocity vector between the fragments) is parallel to $\boldsymbol{R}$. Therefore there will, in general, be a strong correlation between the $\boldsymbol{e}$–$\boldsymbol{\mu}$–$\boldsymbol{R}$–$\boldsymbol{v}$ vectors, and the angular distribution of the photofragments will nearly always be anisotropic.

Another consequence of the anisotropy of the photon absorption is that an alignment or orientation will also be induced in the electronic and rotational angular momentum of the photofragments. This is an $\boldsymbol{e}$–$\boldsymbol{\mu}$–$\boldsymbol{j}$ correlation.[3,17,21] A consequence of this correlation is that if the fragment is produced in an excited state which fluoresces, the emitted light will be polarized whereas if the fragment is produced in its ground state, it will preferentially absorb light of a specific polarization.[2c,17,21b] Actually, since $\boldsymbol{j}$ and $\boldsymbol{v}$ are both correlated to $\boldsymbol{\mu}$, $\boldsymbol{j}$ and $\boldsymbol{v}$ are also correlated independent of $\boldsymbol{e}$. Information concerning these angular momentum correlations can be obtained from the polarization dependence of recoil Doppler-broadened line profiles.[3,5]

As we shall see in the examples presented below, vector properties are often very important in elucidating the dynamics of molecular dissociation. Recently, the importance in this context of interference effects due to simultaneous excitation of several states producing the same final states of the fragments, has been stressed. In the following sections we shall present selected examples that illustrate the influence of these interference effects on vector properties measured in photodissociation experiments. In Section 2 we shall deal with interference phenomena as evidenced in photoejection anisotropy measurements in H_2. In Section 3 the polarization of angular momenta and in particular the orientation of the rotation of a molecular fragment is discussed in relation to some recent experimental and theoretical work on ICN. Finally, in Section 4 we present examples of interference effects in the polarization of the fluorescence during and after the dissociation.

2. Interference Effects on the Photoejection Anisotropy

In spite of the considerable amount of experimental and theoretical work devoted to H_2, the detailed interpretation of the excited-state fragmentation dynamics of this molecule still poses interesting problems. This may seen intriguing since H_2 is the simplest neutral molecule whose adiabatic potentials, at least for the low-lying Rydberg states, are accurately known. However, non-adiabatic interactions and interference effects exist which make the fragmentation dynamics quite subtle.

Recently for instance, it has been shown theoretically[22] and experimentally[23] that partial photodissociation cross-sections into H(2s) + H(1s) and H(2p) + H(1s) present pronounced oscillations as a function of the photon energy when H_2 is excited in the VUV with $\lambda \leqslant 845$ Å. These oscillations are the result of a quantum interference effect between two dissociative pathways obtained by simultaneous excitation of two excited states from the ground state. The two dissociative states are the ($^1\Sigma_u^+$) B and B′ states. In the adiabatic approximation the B state correlates to the H(2p) + H(1s) limit while the B′ state correlates to H(2s) + H(1s). During the half-collision after photon absorption, transitions between the two dissociative channels may occur at large internuclear distances induced by non-adiabatic couplings. The H(2s) + H(1s) final state, for instance, can be obtained by photoabsorption into the B′ state followed by adiabatic dissociation or by photoabsorption into the B state followed by a non-adiabatic transition to the B′ state. Similarly, the H(2p) + H(1s) channel can be produced by photoabsorption into the B state and adiabatic dissociation or absorption into the B′ state followed by a non-adiabatic transition to the B state. Since the two coherently excited pathways lead to the same final state of the fragments, interference results which will be dependent on the relative phases of the continuum wavefunctions in the region of strong coupling. These phases vary differently as a function of energy for the two dissociative states. Hence, the interference contribution to the partial cross-sections oscillates as a function of the photon energy.

A different type of photodissociation experiment involves laser excitation of H_2 prepared initially in the c $^3\Pi_u$ state (see Fig. 1). The c $^3\Pi_u$ state is populated by charge transfer of H_2^+ on Cs vapour. Owing to the Pauli principle for proton exchange, one nuclear spin state for each vibrational and rotational state is metastable and can then be laser-excited to upper dissociative states. A translational spectroscopy technique[4] is used to determine both the released kinetic energy and the angle of dissociation with respect to the laser polarization vector. The amount of energy released for a

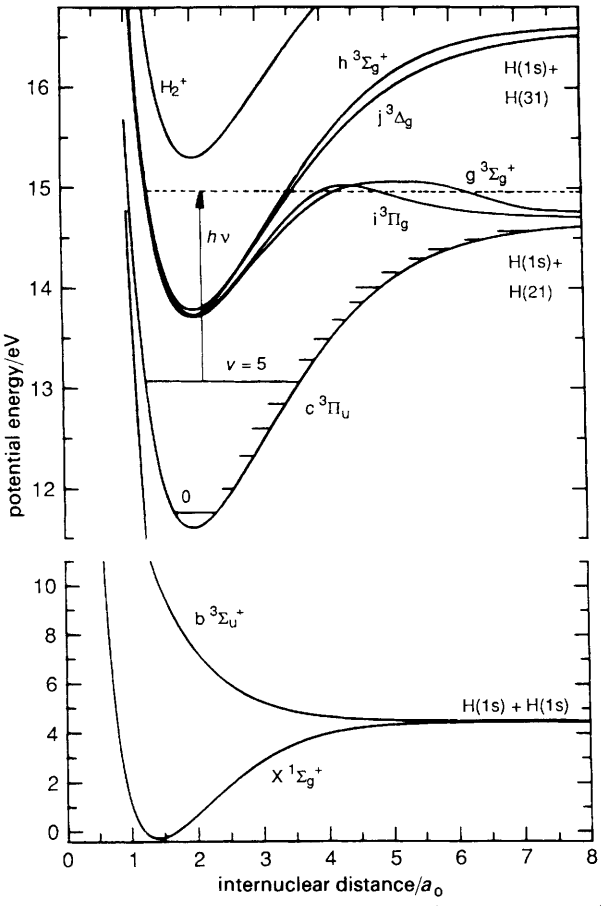

Fig. 1 Relevant potentials of H_2 for the study of resonances associated to the $i\,^3\Pi_g$ state[24]

given laser energy determines the initial rovibrational level of the $c\,^3\Pi_u$ state. In the first example presented here, shape resonances due to the presence of a barrier in the electronic potential are discussed. Secondly, Fano profiles in the photodissociation cross-section will be considered.

A barrier in the electronic potential gives rise to the appearance of quasibound states below the top of the barrier and above the dissociation limit. Excitation to such a quasibound state leads to dissociation by tunnelling of the molecule through the barrier. At specific energies the vibrational continuum wavefunctions have relatively large amplitudes near the region of the minimum in the electronic potential, whereas these amplitudes are much smaller at other energies. This variation of the amplitude shows up as resonances in the photodissociation cross-section. The kinetic energy due to the molecular rotation, *i.e.* the centrifugal potential, also determines the vibrational motion and causes the resonances to appear at different energies for different rotational quantum numbers. For overlapping rotational resonances coherent excitation of the rotational states occurs and gives rise to quantum interference in the differential cross-section. The amount of overlap, and thus the interference, is sensitive to the shape of the barrier in the electronic potential.

As seen in Fig. 1, the adiabatic electronic potential of the $i\,^3\Pi_g$ state of H_2 exhibits a barrier. Photodissociation by tunnelling through this barrier has been investigated by excitation from the $c\,^3\Pi_u$ ($v = 5$, $N = 1$) state to resonances corresponding to the $i\,^3\Pi_g$ ($v' = 5$, $N' = 1$ and $N' = 2$) states,[24] where v' is the vibrational quantum number defined by the number of nodes of the wavefunction behind the barrier, and N' is the rotational quantum number. The $i\,^3\Pi_g$ ($v' = 5$, $N' = 1$, 2) resonances are situated about 300 cm^{-1} below the top of the barrier. The experimentally obtained total photodissociation cross-section as a function of photon energy is presented in Fig. 2. Two partially overlapping resonances are seen at 15 530 and 15 600 cm^{-1} due to excitation to $N' = 1$ and $N' = 2$, respectively.

Theoretically the appearance of these resonances can be understood as follows. The total cross-section is the sum of the squares of the amplitudes of the transition moments $M_{N'}$ for excitation to $N' = 1$ and $N' = 2$,

$$\sigma \propto |M_1|^2 + |M_2|^2 \qquad (1)$$

Since the electronic transition moment is only smoothly varying with the internuclear distance,[25] the right-hand side of eqn. (1) is well approximated by the sum of the Franck–Condon factors for excitation to $N' = 1$ and $N' = 2$, respectively. As mentioned above, the amplitude of the vibrational continuum wavefunction of the $i\,^3\Pi_g$ state varies with energy and is maximum at a resonance. Owing to the centrifugal potential these resonances appear at different energies for $N' = 1$ and $N' = 2$. The sum σ of the calculated Franck–Condon factors in eqn. (1) is given by the solid curve in Fig. 2. The adiabatic potentials of ref. 26 have been used for the $c\,^3\Pi_u$ state and the $i\,^3\Pi_g$ state. Adiabatic corrections, provided by Rychlewski, were added to the potential of the $i\,^3\Pi_g$ state. As can be seen in Fig. 2(*a*), the positions of the two resonances are very well reproduced. However, the calculated relative intensity of the $N' = 2$ resonance is too low.

It is known that non-adiabatic couplings are of great importance in the $n = 3$ Rydberg complex of H_2.[27] If rovibrational couplings among the $N' = 1$ $i\,^3\Pi_g$, $g\,^3\Sigma_g^+$ and $h\,^3\Sigma_g^+$ states are brought into account the calculated cross-section changes only slightly. However, the rotational coupling of the $i\,^3\Pi_g$ ($N' = 2$) state to the $j\,^3\Delta_g$ ($N' = 2$) state, turns out to be much more important. This coupling increases the intensity of the second peak significantly [see Fig. 2(*b*)]. This effect can be described as intensity borrowing of the $i\,^3\Pi_g$ state from the bound $j\,^3\Delta_g$ state. The inclusion of rovibrational couplings has reconciled the experimental and calculated total photodissociation cross-sections.

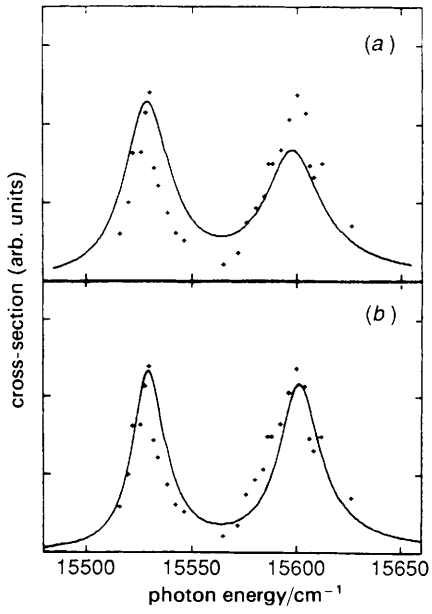

Fig. 2 Experimental and calculated total photodissociation cross-sections of H_2 for excitation around resonances below the top of the barrier in the potential of the $i\,^3\Pi_g$ state. The solid curve in (*a*) is the result of an adiabatic calculation. The solid curve in (*b*) has been obtained by inclusion of rovibrational couplings[24]

The anisotropy parameters β, which characterize the angular dependence of the cross-section according to $\sigma(\theta) \propto 1 + \beta P_2(\cos\theta)$, where P_2 is the second Legendre polynomial, are given in Fig. 3. The anisotropy parameters are seen to change dramatically as the photon energy is scanned over the resonances. Almost all possible values of β, which may take values from -1 to 2, are observed.

From a semi-classical point of view one might have expected the tunnelling probability to increase gradually as the photon energy goes up, since this probability increases as excitation is closer to the top of the barrier.[19] An increasing tunnelling probability corresponds to a faster breakdown of the molecule. In a semi-classical description of the anisotropy one would then expect a β value of 0.5 for slow dissociation far below the top of the barrier,[19] which changes gradually to a value of 2 for axial recoil of the photofragments,[20] resulting from excitation above the barrier. This is in sharp contrast with the experimental observations.

The observed results can be explained only in terms of quantum mechanics and they reflect the coherent excitation of the $i\,^3\Pi_g$ ($N' = 1$) and $i\,^3\Pi_g$ ($N' = 2$) states. Owing to this coherent excitation the product of the transition moments M_1 and M_2 appears in the quantum-mechanical expression of the anisotropy parameter according to

$$\beta = \frac{1}{2} + \frac{3M_1M_2\cos(\delta_1 - \delta_2)}{|M_1|^2 + |M_2|^2} \qquad (2)$$

with δ_1 and δ_2 being the phases of the continuum wavefunctions associated to the $N' = 1$ and $N' = 2$ states. For excitation below the two resonances these phase shifts are almost equal. The transition moments M_1 and M_2 are both small but of almost equal magnitude. According to eqn. (2) this yields an anisotropy parameter close to a value of 2. Note that this value is equal to that for the case of axial recoil, *i.e.* direct fragmentation, for a parallel electronic transition. On approach of the first resonance the magnitude of M_1 increases and the value of δ_1 increases to have changed by π as the resonance has been passed. Near the first resonance the phase shift difference $\delta_1 - \delta_2$ is close to $\pi/2$, giving a β value of 0.5, which is the expected result according to the semi-classical theory of Jonah.[19] This value corresponds to infinite lifetime of the excited state with respect to the rotational period of the molecule. This larger lifetime corresponds to a smaller probability of barrier tunnelling at resonance, reflecting the larger bound character of the excited state at resonance. Experimentally the anisotropy parameter is indeed observed to decrease from a value of 1.0 just below the first resonance to a value of 0.5 at the resonant excitation energy of 15 530 cm^{-1}.

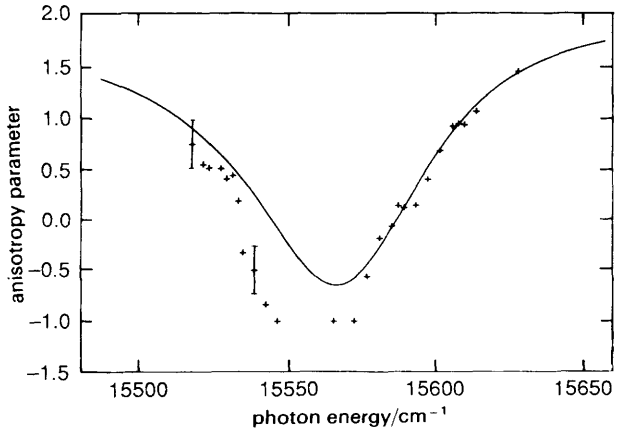

Fig. 3 Experimental and calculated anisotropy parameters for dissociation of H_2 by excitation around resonances below the top of the barrier in the potential of the $i\,^3\Pi_g$ state[24]

In between the two resonances the first resonance has been passed, implying a phase shift difference $\delta_1 - \delta_2$ close to π, whereas the transition moments M_1 and M_2 have almost equal magnitude. According to eqn. (2) this yields an anisotropy parameter close to a value of -1 in between the resonances, as is seen experimentally.

As the photon energy is further increased the second resonance is reached. The phase shift δ_1 does not change significantly, but δ_2 will have changed by π after having passed the second resonance. From the same arguments as above the anisotropy parameter increases to a value of 0.5 near the $N' = 2$ resonance to go further up to a value of 2.0 as the second resonance has been passed. As can be seen in Fig. 3 the observed anisotropy parameters exhibit this behaviour. In Fig. 3 calculated anisotropy parameters including all non-adiabatic couplings are also presented. The agreement with the experimental results is good. Only near 15 500 cm^{-1} are the calculated anisotropy parameters slightly larger than those observed experimentally.

Another type of delayed photodissociation occurs for excitation to a predissociated state, *i.e.* a state which is bound on neglect of a coupling. In this case both the predissociated state and the continuum to which it is coupled can be reached by photon absorption, two indistinguishable pathways are present to the final state. This gives rise to quantum interference. The molecule can either by dissociated by excitation to the predissociated state, which couples to the continuum, or by direct excitation to the continuum. The interference appears as an asymmetry in the energy dependence of the total photodissociation cross-section, which is a Beutler–Fano profile.[28] Furthermore, the anisotropy of the photofragments changes as the energy is scanned over the profile. The width of the profile reflects the magnitude of the coupling between the predissociated state and the continuum. The Fano asymmetry parameter characterizes the shape of the profile and depends upon the ratio of the transition moments for excitation to the predissociated state and the continuum and upon the coupling matrix element, giving rise to predissociation. The Fano asymmetry parameter thus not only provides the relative magnitude of these matrix elements, but also their relative sign. For high absolute values of the Fano asymmetry parameter[28] the interference is difficult to observe in the total cross-section, but is more obviously present in the anisotropy of the photofragments.

Beutler–Fano profiles have been studied in the photodissociation cross-section of H_2.[29,30] Here we will consider only those investigations in which the anisotropy of the photofragments has been observed. Resonances due to those rovibrational $j\,^3\Delta_g$ states that lie in the continuum of the $i\,^3\Pi_g$ state show up as Beutler–Fano profiles in the photodissociation cross-section of H_2 in the metastable $c\,^3H_u$ state. The $j\,^3\Delta_g$ states are predissociative due to the coupling of this state to the $i\,^3\Pi_g$ state by the rotational motion of the nuclei. Both the $j\,^3\Delta_g$ state and the $i\,^3\Pi_g$ state carry oscillator strength from the lower $c\,^3\Pi_u$ state, giving rise to the usual quantum interference in a Beutler–Fano profile.

In Fig. 4 results on the total photodissociation cross-section for excitation from the $c\,^3\Pi_u$ ($v = 5$, $N = 1$) state around the $j\,^3\Delta_g$ ($v' = 5$, $N' = 2$) state are presented. The Fano asymmetry parameter characterizes the total, angle-integrated, cross-section. At the magic angle (*ca.* 55°) with respect to the laser polarization vector, the shape of the energy dependence of the cross-section is equal to that of the total cross-section. The experimentally obtained relative cross-sections at the magic angle for the abovementioned

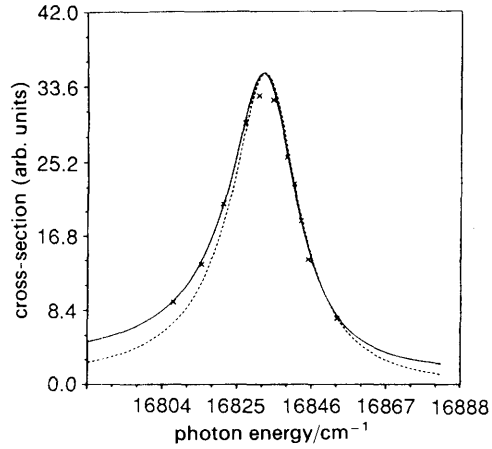

Fig. 4 Experimental photodissociation cross-section for excitation of H_2 from the $c\,^3\Pi_u$ ($v = 5$, $N = 1$) around the resonance due to the $j\,^3\Delta_g$ ($v' = 5$, $N = 2$) state[30]

transition at the magic angle are given in Fig. 4 as function of the photon energy. The curve results from a fit to the experimental results at the magic angle. For comparison the result of a fit at the experimental cross-section for a dissociation angle of 90° is given by the dashed curve. The latter curve is symmetric, as will be explained below. The relative error in the experimental values is about 10% and therefore the asymmetry is not unambiguously observed in the energy dependence of the cross-section at the magic angle only.

In the angular dependence of the cross-section the appearance of interference, *i.e.* asymmetry of the profile, is clearly observed. In Fig. 5 the relative cross-section is given as a function of dissociation angle with respect to the laser polarization vector for three different photon energies. The wiggles in the profiles are systematic errors due to electronic cross-talk in the two particle detectors used. The statistical error is <6%. The angular profiles have been scaled to coincide at a dissociation angle of 90° in order to make the comparison of their shapes easier. The curve obtained with a photon energy of 16 835 cm^{-1} is that for resonant excitation. The curves at 16 815 and 16 853 cm^{-1} are respectively about one level width below and above the resonant excitation energy. It is clear from Fig. 5, that these profiles are different from those at resonance. This is partly due to the fact, that the relative contribution of dissociation *via* the resonance in comparison to that for direct excitation to the continuum is smaller at 16 815 and 16 853 cm^{-1}. However, if this were the only reason for the change of the anisotropy with photon energy, the angular profiles would be the same for excitation at equal distances below and above the resonances. The two off-resonant profiles in Fig. 5, at almost equal distance from the resonance, are different due to the occurrence of interference.

The interference term in the expression of the photodissociation cross-section appears with different signs for excitation below and above the resonance.[28–30] This gives rise to the asymmetry as function of photon energy in both the total cross-section and the angular distribution of the fragments. The terms in the expression of the photodissociation cross-section representing dissociation *via* the resonance and direct excitation to the continuum are the same for excitation at equal energies below and above the resonance. Only the interference term differs in sign and therefore subtraction of the profiles at 16 853 and 16 815 cm^{-1} gives the angular dependence of the interference term. The result of this subtraction, or the interference term, is presented in Fig. 6. It is clearly seen that the interference term is different from zero and its importance increases at smaller dissociation angles. The profile in Fig. 6 gives the sign of the Fano asymmetry parameter, which is seen to be negative for the considered transition.

From Fig. 6 it is also seen that the interference term vanishes at a dissociation angle of 90°, resulting in a symmetric Lorentzian-shaped energy dependence of the total cross-section. As has been mentioned above, the result of a fit to the experimental total cross-section at a dissociation angle of 90° is given in Fig. 4 and is symmetrical to within the experimental error. The interference term vanishes at a dissociation angle of 90° due to the parallel character of the photon excitation from the $c\,^3\Pi_u$ state to the $i\,^3\Pi_g$ state. This Π–Π transition gives a $\cos^2\theta$ dependence of the angular distribution, which is zero at a dissociation angle of 90°. The disappearance of the direct excitation to the continuum of the $i\,^3\Pi_g$ state at 90° makes the dissociation *via* the resonance due to the $j\,^3\Delta_g$ state the only possible pathway at this angle, resulting in a symmetrical Lorentzian profile.

The experimental results on both the energy and angular dependence of the cross-section for excitation around several resonances due to the $j\,^3\Delta_g$ state have been reproduced by those from *ab initio* calculations.[30] The results show that

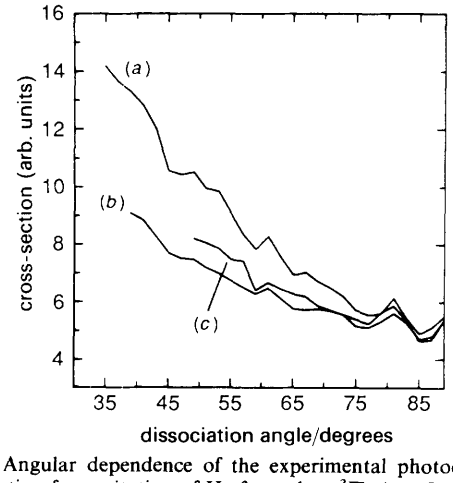

Fig. 5 Angular dependence of the experimental photodissociation cross-section for excitation of H_2 from the $c\,^3\Pi_u$ ($v = 5$, $N = 1$) state to the $j\,^3\Delta_g$ ($v' = 5$, $N' = 1$) resonance with photon energies of: (*a*) 16 815 cm^{-1}, (*b*) 16 835 cm^{-1}, (*c*) 16 853 cm^{-1}. The profiles have been scaled to coincide at 90°[30]

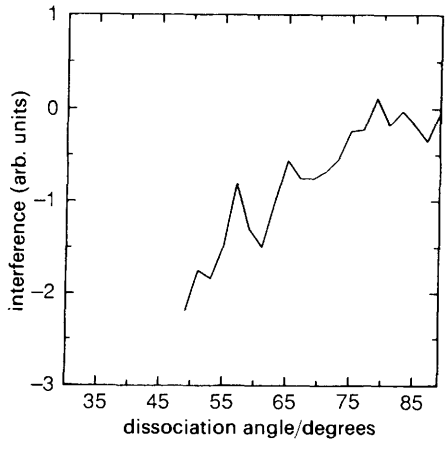

Fig. 6 Angular dependence of the interference term in the Beutler–Fano profile in the photodissociation cross-section for excitation from the $c\,^3\Pi_u$ ($v = 5$, $N = 1$) state to the $j\,^3\Delta_g$ ($v' = 5$, $N' = 2$) resonance[30]

interference plays an important role in the angular dependence of the photodissociation cross-section.

3. Polarization of Photofragment Angular Momenta

Alignment and orientation of product angular momenta is often referred to as product polarization, *e.g.* polarized electrons in photoemission experiments.[31] The degree of polarization of a particular product measures the correlation or anisotropy of the angular momentum vector $\boldsymbol{j}$ of that product with respect to some laboratory axis. In the case of photofragmentation this axis is defined by the incident photon, *i.e.* by the direction of its electric field in the case of linear incident polarization or by its propagation direction in the case of circular photon polarization.

Quantum mechanically, the degree of product polarization is determined by the distribution of the population of m_j sublevels associated to the projections of $\boldsymbol{j}$ on the space-fixed axis. The degree of orientation $\mathcal{O}$ for instance (also denoted $A_0^{(1)}$ in the literature[17,21]), is defined by the first moment of that distribution,

$$\mathcal{O}^{(j)} \equiv \langle j_z/|\boldsymbol{j}|\rangle = \sum_{m_j} \frac{m_j}{\sqrt{[j(j+1)]}}\, \rho^{(j)}_{m_j, m_j} \qquad (3)$$

where $\rho^{(j)}_{m_j, m_j}$ is the final relative population of sublevel m_j with $\sum_{m_j} \rho^{(j)}_{m_j, m_j} = 1$. The degree of orientation alignment (also denoted $A_0^{(2)}$) is defined by the second moment (bipolar moment),

$$\mathcal{A}^{(j)} \equiv \langle 3j_z^2/|\boldsymbol{j}|^2 - 1\rangle = \sum_{m_j} \left(\frac{3m_j^2}{j(j+1)} - 1\right)\rho^{(j)}_{m_j, m_j} \qquad (4)$$

From eqn. (3) it is clear that the degree of orientation is zero when $\rho^{(j)}_{m_j, m_j} = \rho^{(j)}_{-m_j, -m_j}$, *i.e.* when the population distribution is symmetric with respect to 0. Geometrical considerations indicate that linearly polarized light cannot break the positive/negative symmetry. Hence orientation of photofragments can be obtained only through the use of circularly polarized light, a property which is well known in the context of photoionization.[21,31]

In molecular photofragmentation several measurements[32] have been conducted on the degree of alignment of fragments angular momenta by the use of linearly polarized light, but very few have dealt with orientation. The first evidence for orientation of atomic fragments in the dissociation of diatomic molecules has been given by Vasyutinskii.[33] The oriented ground-state caesium atoms produced in the photodissociation of CsI molecules by circularly polarized UV radiation were monitored by optical dichroism. More recently, oriented ground-state Tl atoms were produced by dissociating TlBr and in this case it has been shown that nonadiabatic effects in the excited electronic states have a profound influence on the degree of orientation.[34]

In the photodissociation of diatomic molecules it is the alignment and orientation of the fragments electronic angular momenta which is produced. Only very recently, orientation of a rotational angular momentum in a molecular photofragment has been observed.[35] By photolysing ICN with circularly polarized light, Zare and co-workers have produced oriented CN($X\,^2\Sigma^+$, v, N) fragments for N in the range 1–60. This is very different from the situation in the case of diatomic molecules where the electronic angular momentum never exceeds a few units, and allows the study of the classical limit $N \gg 1$. In the ICN experiments, it was found that the degree and sign of the orientation changes as a function of the rotational state N being considered. For low N states the orientation is positive but for large N it becomes negative. It has been noted by Vigué *et al.*[36] that the degree of orientation found in these experiments for large N correspond to an average value of $|\langle N_z\rangle| \approx 7$, which is much larger than the unit angular momentum transferred to the molecule by the photon. An elegant model has been proposed by these authors to explain this unexpected result. The excited dissociative state (which corresponds to a Σ state in the collinear configuration) is assumed to acquire some mixed Π character due to the coupling with another state in the same energy region. The coupling is obviously zero at the collinear configuration but non-zero as the molecule bends. As a result of the mixing, it is possible to excite a coherent superposition of the $v = 0$ and $v = 1$ bending states which corresponds to a preferred sense of the rotation of CN within the ICN complex. This effect has been described as a vibronic angular momentum 'amplification'.[36]

A general quantum treatment for the production of a significant orientation of fragments in highly excited rotational states has been considered recently.[37] This involves the coherent excitation of at least two dissociative states with different helicities Ω (projection of $\boldsymbol{N}$ on the axis joining the centres of mass of the fragments), correlating to the same final state of the fragments. In the simple case of only three components $\Omega = 0, \pm 1$, it is obtained in the limit of $N \gg 1$

$$\mathcal{O}^{(N)} = \mp \frac{1}{2}\left(\frac{M_0^{(N)*}M_{1(+)}^{(N)} + M_0^{(N)}M_{1(+)}^{(N)*}}{|M_0^{(N)}|^2 + |M_{1(+)}^{(N)}|^2 + |M_{1(-)}^{(N)}|^2}\right) \qquad (5)$$

where the two signs refer to right and left polarization, respectively. In eqn. (5) the $M_0^{(N)}$ and $M_{1(\pm)}^{(N)}$ are the dissociation amplitudes for the production of fragments in the rotational state N with projection 0 and 1 on the reaction axis (the superscripts ± 1 indicate parity with respect to the plane of the molecule. It is clear from eqn. (5) that in the limit $N \gg 1$ considered here, orientation can be obtained only if two helicity states are excited simultaneously. Actually, only $M_0^{(N)}$ and $M_{1(+)}^{(N)}$ are necessary and not $M_{1(-)}^{(N)}$. This corresponds to the excitation of two parallel transitions, *i.e.* the transition dipole moments are both on the plane of the molecule. From eqn. (5) we also note that the orientation can be as large as 1/2 for $M_0^{(N)} = M_{1(+)}^{(N)}$ and $M_{1(-)}^{(N)} = 0$. Since $\langle N_Z\rangle = N\mathcal{O}^{(N)}$ and $N \gg 1$, we can then obtain $|\langle N_Z\rangle| \gg 1$.

It is also interesting to analyse the alignment in the limit $N \gg 1$. For linear incident polarization, we obtain

$$\mathcal{A}^{(N)} = -\frac{2}{5}\left(\frac{|M_0^{(N)}|^2 + |M_{1(+)}^{(N)}|^2 - 2|M_{1(-)}^{(N)}|^2}{|M_0^{(N)}|^2 + |M_{1(+)}^{(N)}|^2 + |M_{1(-)}^{(N)}|^2}\right) \qquad (6)$$

and we find that $\mathcal{A}^{(N)} = -2/5$ if $M_{1(-)}^{(N)} = 0$, while $\mathcal{A}^{(N)} = 4/5$ if $M_0{}^{(N)} = M_{1(+)}^{(N)} = 0$, which are the limiting values of the alignment.[17,38] This result is also expected in the framework of the classical model.[39] Since $N \gg 1$, then if the initial overall rotational angular momentum is small as compared to N, we shall have N perpendicular to the plane of the molecule. Now for large N, $M_0^{(N)}$ and $M_{1(+)}^{(N)}$ correspond to parallel transitions, *i.e.* to a transition dipole moment in the plane of the molecule, while $M_{1(-)}^{(N)}$ correspond to a transition dipole moment along $\boldsymbol{N}$. We shall then have for linear polarization along the laboratory Z-axis

$$\boldsymbol{M}\cdot\hat{\boldsymbol{e}} = M_0^{(N)}\cos\Theta + M_{1(+)}^{(N)}\sin\Theta\cos\Phi + M_{1(-)}^{(N)}\sin\Theta\sin\Phi \qquad (1)$$

and the absorption probability will be

$$dW_{abs} = \frac{3}{4\pi}\frac{\left|M_0^{(N)}\cos\Theta + M_{1(+)}^{(N)}\sin\Theta \times\cos\Phi + M_{1(-)}^{(N)}\sin\Theta\sin\Phi\right|^2}{|M_0^{(N)}|^2 + |M_{1(+)}^{(N)}|^2 + |M_{1(-)}^{(N)}|^2}\, d(\cos\Theta)\, d\Phi \qquad (8)$$

Since $\mathscr{A}^{(N)} = \langle 3N_z^2/N^2 - 1 \rangle$ and in the classical limit $N_Z = N \sin\Theta \sin\Phi$, one obtains

$$\mathscr{A}^{(N)} = 3 \int \mathrm{d}W_{\mathrm{abs}} \sin^2\Theta \sin^2\Phi - 1$$

$$= -\frac{2}{5}\left(\frac{|M_0^{(N)}|^2 + |M_{1(+)}^{(N)}|^2 - 2|M_{1(-)}^{(N)}|^2}{|M_0^{(N)}|^2 + |M_{1(+)}^{(N)}|^2 + |M_{1(-)}^{(N)}|^2}\right) \quad (9)$$

which is exactly the result obtained in eqn. (6) using the quantum formalism. On the other hand, eqn. (5) shows that even in the classical limit ($N \gg 1$) the orientation depends on the relative phases of the dissociative wavefunctions. This quantum interference effect is not present in the alignment.

Very recently Yabushita and Morokuma[40] have performed *ab initio* calculations for the ICN molecule in the ground and in several excited electronic states. Based on these calculations they have proposed that two of their calculated excited electronic states (the $^3\Pi_0^+$ and $^1\Pi_1$ states), both of them optically active from the ground state, should be directly involved in the dissociation of ICN in the A continuum (see Fig. 7). The two excited surfaces are bent and they undergo a conical intersection in the exit valley outside the Franck–Condon region. Since the two electronic states are coupled and have different symmetry, it is possible to excite two helicity states for each final state of the fragments. Thus, according to the general theory[37] the Yabushita and Morokuma potential scheme should also be able to explain the orientation of rotationally excited CN fragments found in the ICN experiment. Recently,[37b] quantum close-coupling calculations using these potentials have been performed. The rotational distribution of the CN fragments calculated at the excitation energy of the experiments is presented in Fig. 8. Very good agreement between theory and experiments is obtained. The calculated orientation of the CN rotational angular momentum is presented in Fig. 9, together with the measured values. The agreement is not as good but the overall trend is reproduced, in particular the change of sign. These results clearly show that orientation is more sensitive to the exact form of the potential-energy surfaces and couplings than the rotational distribution and this is due again to the contribution of interference effects. These calculations also demonstrate that the degree of orientation can be unexpectedly large if two or more helicity continua correlating to the same final states of the fragments are excited simultaneously. The helicity is associated to the projection Ω of $\boldsymbol{j}$ onto the dissociation coordinate $\boldsymbol{R}$ joining the centre of mass of the fragments. The simultaneous excitation of continua with different helicity can be achieved in many different ways.

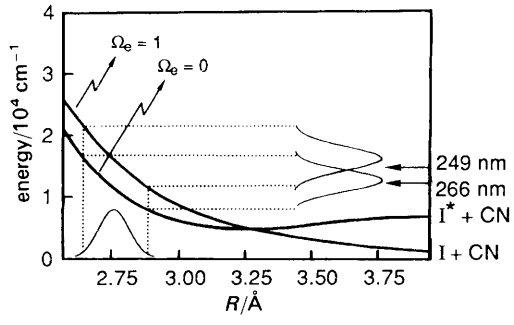

Fig. 7 Excited-state potential-energy curves for ICN in the collinear configuration for the two-state model. The curves are represented as a function of the distance R between the centre of mass of CN and the iodine atom for a fixed CN distance of 1.17 Å. Also represented is the ground-state wavefunction and the corresponding partial photodissociation cross-sections for the two channels in the collinear configuration

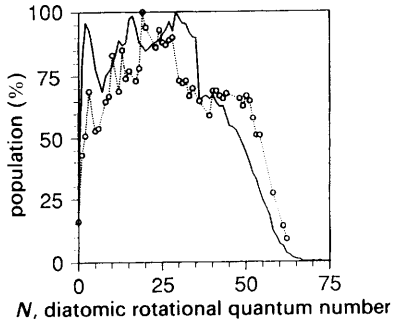

Fig. 8 CN final-state rotational distribution following photodissociation of ICN at 249 nm. The solid line represents the theoretical results obtained with the two-state model. The points are the experimental relative populations measured by O'Halloran *et al.*[35a]

If only one excited electronic manifold is populated then in the framework of the Franck–Condon approximation we require that the transition dipole moment should have parallel and perpendicular components onto $\boldsymbol{R}$. For non-linear molecules this is likely to be the rule. For a bent triatomic molecule for instance, the transition dipole moment should be in the plane of the molecule forming an angle different from 0 and $\pi/2$ with respect to $\boldsymbol{R}$. A typical example is provided by NOCl which in the region 620–180 nm has transition dipole moments very nearly parallel to the NCl bond.[41]

For linear molecules (such as ICN), it is clear that the transition dipole moment lies parallel or perpendicular to $\boldsymbol{R}$ in the collinear configuration. Hence with only one surface orientation for large j can only be obtained through mixing with another surface of different symmetry. This mixing can exist only out of the collinear configuration and thus for linear molecules it is the contribution of the zero-point bending vibration of the ground state which is responsible for the orientation. This is the mechanism discussed by Vigué *et al.*[36] Other possible mechanisms for linear triatomic molecules if two excited electronic states with different symmetry (one parallel and the other one perpendicular) are optically connected to the ground state, simultaneous excitation of two helicity states can be obtained (provided the Franck–Condon factors are favourable). This is the situation encountered in the two-state model of ICN advanced by Morokuma and Nabushita.[40] Although the two states are correlated to different final states of the fragments (I + CN and I* + CN), transitions can occur in the crossing region when the molecule is bent. This ensures that the same final state of the fragments can be obtained with two different helicity states. The two-state model of Morokuma and Yabushita[40] and the mixing

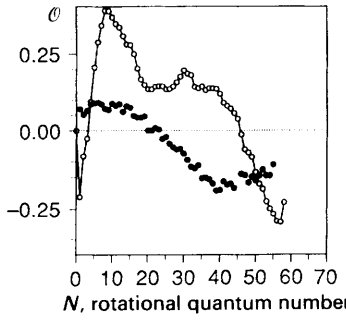

Fig. 9 Degree of orientation of the rotational angular momentum N of the CN fragments *vs.* N. The theoretical results (solid line) correspond to the two-state model calculations. The experimental points (in black) are those of Hasselbrink *et al.*[35b]

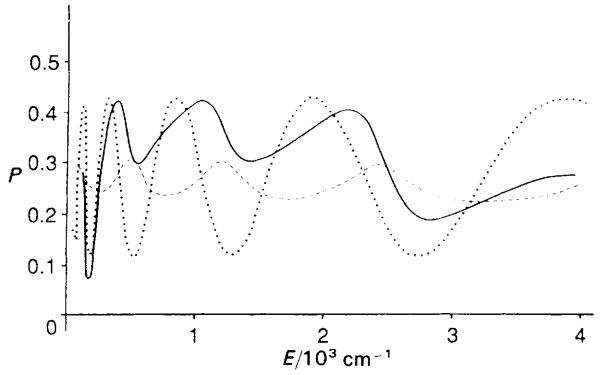

Fig. 10 Predicted polarization of the Ly_α emission following photodissociation of H_2. The full calculation including all couplings is represented by the solid curve. The dotted curve corresponds to a calculation in which the non-adiabatic coupling between the B and B′ states is neglected, while the dashed curve is the result obtained when the coherence excitation of the Σ and Π states is ignored

mechanism advanced by Vigué *et al.*,[36] are in fact intimately connected. If the crossing point between the two surfaces occurs near the Franck–Condon region, the adiabatic surfaces will then have the mixed transition dipole moment assumed by Vigué *et al.* This situation is likely to be found in many systems.

4. Fluorescence

Since the pioneering theoretical prediction by van Brunt and Zare[41] in 1968, several experimental and theoretical studies have dealt with polarization of the light emitted by photofragments.[42–50] Recently, the importance of coherence effects on the degree of polarization has been emphasized.[48–50] One particularly striking example is provided by the photodissociation of Ca_2 into Ca*(P) + Ca(S) *via* the excitation of its first dissociative Π state.[48] Since the projection of the electronic angular momentum on the internuclear axis is $\Lambda = \pm 1$ for a Π state, the excited Ca*(P) atom will be produced in the magnetic sublevels ± 1 if the dissociation proceeds adiabatically. Thus the Ca* atom is fully aligned in the molecular frame and it will be still partially aligned with respect to the space-fixed frame after averaging over the absorption probability. For linearly polarized incident light, the degree of polarization is given in the classical model by

$$\mathscr{P} \equiv \frac{I_{\parallel} - I_{\perp}}{I_{\parallel} + I_{\perp}} = \frac{3\langle\cos^2\alpha\rangle - 1}{2 + 3\langle\cos^2\alpha\rangle} \qquad (10)$$

where α is the angle between the absorbing and emitting dipoles. For the Ca_2 case, eqn. (10) predicts $\mathscr{P} = 0.14$, while the experimental value is $\mathscr{P} = 0.64$. Not only is the disagreement large but in addition the measured value is beyond the maximum classical value of $\mathscr{P} = 0.5$ [see eqn. (10)]. This, at first sight, surprising result has been explained as due to the interference between the emission from the magnetic sublevels ± 1 coherently populated in the dissociation of a Π molecular state. When this coherence is taken into account the quantum calculation gives $\mathscr{P} = 0.78$ in reasonably good agreement with the experiment, but when the interference contributions are neglected the polarization drops to $\mathscr{P} = 0.14$ which is exactly the value predicted by the classical model.

Other types of coherence effects can be produced in the populations of the magnetic sublevels.[50] Consider for example the case discussed above, namely the AB molecule dissociation into A*(^{1}P) + B(^{1}S) fragments. Two molecular singlet states ($^1\Pi$ and $^1\Sigma$) are correlated to this limit. They can both be populated by optical absorption from the $^1\Sigma$ ground state and therefore they will be coherently excited. Since adiabatically the $^1\Pi$ state is correlated to A*(^{1}P, $m = \pm 1$) fragments and the $^1\Sigma$ state to A*(^{1}P, $m = 0$) fragments, the photodissociation will induce an additional coherence between the $m = 0$ and the $m = \pm 1$ magnetic sublevels. As opposed to the case discussed above, this coherence depends on the ratio of photoabsorption amplitudes for excitation of the $^1\Sigma$ and $^1\Pi$ dissociative states as well as on the relative phases of their corresponding vibrational continuum wavefunctions.

Recently,[50] a quantum-mechanical calculation of the degree of polarization of emission in the photodissociation of H_2 leading to H(1s) + H(2p) fragments, has been completed. The calculation of the photodissociation amplitudes was performed by integration of the time-independent close-coupled Schrödinger equations for the B($^1\Sigma$), B′($^1\Sigma$) and C($^1\Pi$) electronic states of H_2, using the existing *ab initio* potential-energy curves, adiabatic corrections, non-adiabatic couplings, and transition dipole moments. The photodissociation amplitudes were in turn used to calculate the polarization degree of the fluorescence. It was shown that coherence effects can produce pronounced oscillations of the fluorescence polarization as a function of the photon energy (see Fig. 10). The polarization degree can be written as

$$\mathscr{P} = \frac{6|A_\Sigma|^2 + 2|A_\Pi|^2 + 9(A_\Sigma A_\Pi^* + (A_\Sigma^* A_\Pi)}{32|A_\Sigma|^2 + 67|A_\Pi|^2 + 3(A_\Sigma A_\Pi^* + (A_\Sigma^* A_\Pi)} \qquad (11)$$

Two interference effects are present simultaneously in the H_2 case. There is an interference between the simultaneous excitation of the B and B′ Σ states which produces an oscillating behaviour of A_Σ according to

$$A_\Sigma \propto A_B \exp(i\phi_B) + A_{B'} \exp(i\phi_{B'}) \qquad (12)$$

In addition the coherent excitation of the B and C states contributes with an additional interference term involving the products of A_Σ and A_Π in eqn. (11).

Interference effects can also dramatically affect the spatial anisotropy and the polarization of emitted photons during the dissociative half-collision. The technique of emission spectroscopy of dissociating molecules has developed greatly in the last years.[51–53] It provides a complementary probe of the nuclear dynamics between the Franck–Condon region accessed by the photon excitation and the asymptotic region of the products. In a time-dependent description, as the molecule evolves on the repulsive excited surface it may emit photons by optical transitions to the excited vibrational levels of the ground state.[54] Thus, this process could be described as Raman scattering from dissociative continua.[55] Recently polarized emission spectroscopy in which the anisotropic distribution of photons emitted during dissociation is also monitored[52–53] has been applied to CH_3NO_2 and CH_3I. The excitation simultaneously promotes the molecule to two coupled excited electronic surfaces. It has been demonstrated that the contributions of the interference terms and information on the electronic non-adiabatic coupling, can be extracted from the polarized emission spectrum by determining the three linearly independent contributions to the scattering intensity.

5. Conclusions

We have presented selected examples demonstrating the importance of interference effects on vector properties of molecular photofragmentation such as the angular distributions and orientation of the photoproducts, as well as on the

anisotropy of the emitted fluorescence during and after the dissociation. These effects are due to the simultaneous excitation of two or more fragmentation pathways leading to the same final state of the fragments.

At the excitation energies of visible and UV experiments usually many molecular electronic states lie close together. A detailed knowledge of the number of excited states involved in the excitation process and subsequent evolution, and the shapes of their associated potential-energy surfaces and couplings, is needed in order to understand excited-state dynamics. In bound–bound spectroscopy, high-resolution spectra and quantum chemistry calculations usually provide sufficient information to be able to describe the excited-state manifold in the Franck–Condon region. In photofragmentation processes, however, the potentials and their couplings at larger internuclear distances also play an important role and the inversion problem is much more involved. Hence, scalar properties are usually not enough for a complete understanding of the photodissociation dynamics.

We have shown that detailed quantum analysis of the interference contributions on vector properties can provide basic information on excited potential-energy surfaces, couplings, and in general, on the mechanisms of the photofragmentation dynamics. This also implies that quantum simulations are important for a complete understanding of photodissociation experiments.

In the future, several experimental and theoretical developments are likely to occur. Ultrashort pulses could be used to monitor the vector properties in real time.[56] It should be noted in this context that this will imply high-intensity pulses. Therefore the study of high-field effects on the photodissociation dynamics will be of importance. Another, very exciting field for future developments concerns the use of van der Waals complexes to study directional photodissociation.[57] These experiments, in which a molecule embedded in a complex or cluster is photodissociated, are related to similar problems of photodissociation of molecules on surfaces, matrices or liquids.[58]

The work on the angular distributions of the photofragments of molecular hydrogen is part of the research program of the Stichting voor Fundamenteel Onderzoek der Materie (Foundation for the Fundamental Research on Matter) and was made possible by the financial support of the Nederlandse Organisatie voor Wetenschappelijk Onderzoek (Netherlands Organization for the Advancement of Research).

References

1 R. Schinke, *Photodissociation Dynamics: Molecular Motion in Excited States*, Wiley, New York, 1992; M. Shapiro and G. G. Balint-Kurti, *Chem. Phys.*, 1981, **61**, 137; M. Shapiro and G. G. Balint-Kurti, in *Photodissociation and Photoionization*, ed. K. P. Lawley, Wiley, New York, 1985; R. Schinke, *Annu. Rev. Phys. Chem.*, 1988, **39**, 39.

2 S. R. Leone, *Annu. Rev. Phys. Chem.*, 1984, **35**, 109; F. F. Crim, *Annu. Rev. Phys. Chem.*, 1984, **35**, 657; J. P. Simons, *J. Phys. Chem.*, 1984, **88**, 1287.

3 H. Reisler and C. Wittig, *Annu. Rev. Phys. Chem.*, 1986, **37**, 307; P. L. Houston, *J. Phys. Chem.*, 1987, **91**, 5388; J. P. Simons, *J. Phys. Chem.*, 1987, **91**, 5378; G. E. Hall and P. L. Houston, *Annu. Rev. Phys. Chem.*, 1989, **40**, 375.

4 D. P. de Bruijn and J. Los, *Rev. Sci. Instrum.*, 1982, **53**, 1020.

5 R. N. Zare, *Ber. Bunsenges. Phys. Chem.*, 1982, **86**, 422; R. Vasudev, R. N. Zare and R. N. Dixon, *J. Chem. Phys.*, 1984, **80**, 4863; R. N. Dixon, *J. Chem. Phys.*, 1986, **85**, 1866; U. Hefter, G. Ziegler, A. Mattheus, A. Fisher and K. Bergmann, *J. Chem. Phys.*, 1986, **85**, 286; M. Brouard, M. T. Martinez, J. O'Mahoney and J. P. Simons, *Mol. Phys.*, 1990, **69**, 65.

6 A. H. Zewail, *Science*, 1988, **242**, 1645; M. Gruebele and A. H. Zewail, *Phys. Today*, May 1990; L. R. Khundkar and A. H. Zewail, *Annu. Rev. Phys. Chem.*, 1990, **41**, 15.

7 K. C. Janda and C. R. Bieler, in *Atomic and Molecular Clusters*, ed. R. B. Bernstein, Elsevier, Amsterdam, 1990, p. 455; see also *Dynamics of Polyatomic van der Waals Complexes*, ed. N. Halberstadt and K. C. Janda, NATO ASI Series B, Plenum Press, New York, vol. 227, 1990.

8 C. Jouvet and B. Soep, *J. Chem. Phys.*, 1984, **80**, 2229; S. Buelow, G. Radhakrishnan, J. Catanzarite and C. Wittig, *J. Chem. Phys.*, 1985, **83**, 444; S. K. Shin, Y. Chen, S. Nikolaisen, S. W. Sharpe, R. A. Beaudet and C. Wittig, *Adv. Photochem.*, July 1990.

9 F. F. Crim, in *Molecular Photodissociation Dynamics*, *Advances in Gas-Phase Photochemistry and Kinetics*, ed. M. N. R. Ashfold and J. E. Baggott, Royal Society of Chemistry, London, 1987, p. 177.

10 K. H. Kramer and R. B. Bernstein, *J. Chem. Phys.*, 1965, **42**, 767; P. R. Brooks, *Science*, 1976, **193**, 11; B. Friedrich and D. Herschbach, *Nature (London)*, 1991, **353**, 412; P. A. Block, E. J. Bohac and R. E. Miller, to be published.

11 G. Herzberg, *Molecular Spectra and Molecular Structure, I. Spectra of Diatomic Molecules*, Van Nostrand Reinhold, New York, 1950.

12 H. Lefebvre-Brion and R. W. Field, in *Perturbations in the Spectra of Diatomic Molecules*, Academic Press, New York, 1986.

13 J. A. Beswick and J. Jortner, *Adv. Chem. Phys.*, 1981, **47**, 363.

14 S. Mukamel and J. Jortner, *J. Chem. Phys.*, 1974, **61**, 227; *J. Chem. Phys.*, 1976, **65**, 3735.

15 E. J. Heller, *J. Chem. Phys.*, 1978, **68**, 2066; K. C. Kulander and E. J. Heller, *J. Chem. Phys.*, 1978, **69**, 2439; S. O. Williams and D. G. Imre, *J. Phys. Chem.*, 1988, **92**, 6648; J. A. Beswick and J. Jortner, *Chem. Phys. Lett.*, 1990, **168**, 246.

16 See contributions and references in Proceedings of Faraday Symposium 24, 1989, *J. Chem. Soc., Faraday Trans. 2*, 1989, **85** (8).

17 C. H. Greene and R. N. Zare, *Annu. Rev. Phys. Chem.*, 1982, **33**, 119.

18 R. N. Zare and D. R. Hershbach, *Proc. IEEE*, 1963, **51**, 173.

19 C. Jonah, *J. Chem. Phys.*, 1971, **55**, 1915.

20 R. N. Zare, *Mol. Photochem.*, 1972, **4**, 1.

21 K. Blum, *Density Matrix Theory and Applications*, Plenum Press, New York, 1981; U. Fano and J. H. Macek, *Rev. Mod. Phys.*, 1973, bf. 45, 553.

22 J. A. Beswick and M. Glass-Maujean, *Phys. Rev. A*, 1987, **35**, 3339.

23 M. Glass-Maujean, H. Frohlich and J. A. Beswick, *Phys. Rev. Lett.*, 1988, **61**, 157.

24 L. D. A. Siebbeles, J. M. Schins, W. J. van der Zande, J. Los and M. Glass-Maujean, *Phys. Rev. A*, 1991, **44**, 343.

25 J. M. Schins, L. D. A. Siebbeles, W. J. van der Zande, J. Los, H. Koch and J. Rychlewski, *Phys. Rev. A*, 1991, **44**, 4171.

26 W. Kolos and J. Rychlewski, *J. Mol. Spectrosc.*, 1977, **66**, 428.

27 J. M. Schins, L. D. A. Siebbeles, W. J. van der Zande and J. Los, *Phys. Rev. A*, 1991, **44**, 4161.

28 U. Fano, *Nuovo Cimento*, 1935, **12**, 56; U. Fano, *Phys. Rev.*, 1961, **124**, 1866.

29 L. D. A. Siebbeles, J. M. Schins and J. Los, *Phys. Rev. Lett.*, 1990, **46**, 1514.

30 L. D. A. Siebbeles, J. M. Schins, J. Los and M. Glass-Maujean, *Phys. Rev. A*, 1991, **44**, 1584 and references therein.

31 N. A. Cherepkov, *Adv. Atom Molec. Phys.*, 1983, **19**, 395; U. Heinzmann, in *Applications of Circularly Polarized Radiation using Synchrotron Radiation and Ordinary Sources*, ed. F. Allen and C. Bustamante, Plenum Press, New York, 1985.

32 P. Andresen, G. S. Ondrey, B. Titze and E. Rothe, *J. Chem. Phys.*, 1984, **80**, 2548; O. Benoist d'Azy, F. Lahmani, C. Lardeux and D. Solgadi, *Chem. Phys.*, 1985, **94**, 247; D. Schwartz-Lavi, I. Bar and S. Rosenwaks, *Chem. Phys. Lett.*, 1986, **128**, 123; Y. Y. Bai, A. Ogai, C. X. W. Qian, L. Iwata, G. A. Segal and H. Reisler, *J. Chem. Phys.*, 1989, **90**, 3903; E. A. J. Wannenmacher, H. Lin, W. H. Fink, A. J. Paul and W. M. Jackson, *J. Chem. Phys.*, 1991, **95**, 3431.

33 O. S. Vasyutinskii, *Sov. Phys. JETP Lett.*, 1980, **31**, 428; *Opt. Spectrosc. (U.S.S.R.)*, 1980, **51**, 124.

34 O. S. Vasytinskii, *Z. Phys. D*, 1990, **15**, 105.

35 (*a*) O'Halloran, H. Joswig and R. N. Zare, *J. Chem. Phys.*, 1987, **87**, 303; (*b*) E. Hasselbrink, J. R. Waldeck and R. N. Zare, *Chem. Phys.*, 1988, **126**, 191.

36 J. Vigué, B. Girard, G. Gouédard and N. Billy, *Phys. Rev. Lett.*, 1989, **62**, 1358.
37 (*a*) M. Glass-Maujean and J. A. Beswick, *J. Chem. Soc., Faraday Trans. 2*, 1989, **85**, 983; (*b*) J. A. Beswick, M. Glass-Maujean and O. Roncero, *J. Chem. Phys.*, in the press.
38 R. N. Zare, *Angular Momentum: Understanding Spatial Aspects in Chemistry and Physics*, Addison Wesley, New York, 1988.
39 G. A. Chamberlain and J. P. Simons, *Chem. Phys. Lett.*, 1975, **32**, 355; *J. Chem. Soc., Faraday Trans. 2*, 1975, **71**, 2043.
40 S. Yabushita and K. Morokuma, *Chem. Phys. Lett.*, 1990, **175**, 518.
41 R. J. van Brunt and R. N. Zare, *J. Chem. Phys.*, 1968, **48** 4304.
42 M. MacPherson and J. P. Simons, *J. Chem. Soc., Faraday Trans. 2*, 1979, **75**, 1572.
43 E. D. Poliakoff, S. H. Southworth, D. A. Shirley, K. H. Jackson and R. N. Zare, *Chem. Phys. Lett.*, 1979, **65**, 407.
44 E. W. Rothe, U. Krause and R. Duren, *Chem. Phys. Lett.*, 1980, **72a**, 100.
45 J. Husain, J. R. Wiesenfeld and R. N. Zare, *J. Chem. Phys.*, 1980, **72**, 2479; G. W. Loge and R. N. Zare, *Mol. Phys.*, 1981, **43**, 1419; G. W. Loge and J. R. Wiesenfeld, *Chem. Phys. Lett.*, 181, **78**, 32.
46 E. D. Poliakoff, J. L. Dehmer, D. Dill, A. C. Parr, D. H. Jackson and R. N. Zare, *Phys. Rev. Lett.*, 1981, **46**, 907.
47 O. S. Vasyutinskii, *Sov. Phys. JETP*, 1981, **54**, 855; *Zh. Eksp. Teor. Fiz.*, 1981, **81**, 1608; *Khim. Phys.*, 1986, **5**, 768.
48 J. Vigué, P. Grangier, G. Roger and A. Aspect, *J. Phys. Lett.*, 1981, **42**, 531; J. Vigué, J. A. Beswick, and M. Broyer, *J. Phys. (Paris)*, 1983, **44**, 1225.
49 S. J. Singer, K. F. Freed and Y. B. Band, *J. Chem. Phys.*, 1983, **79**, 6060; Y. B. Band, K. F. Freed and S. J. Singer, *J. Chem. Phys.*, 1986, **84**, 3762.
50 M. Glass-Maujean and J. A. Beswick, *Phys. Rev. A*, 1987, **36**, 1160; M. Glass-Maujean and J. A. Beswick, *Phys. Rev. A*, 1988, **38**, 5660.
51 D. G. Imre, J. L. Kinsey, A. Sinha and J. Krenos, *J. Chem. Phys.*, 1984, **88**, 3956.
52 K. Q. Lao, M. D. Person, P. Xayariboum and L. J. Butler, *J. Chem. Phys.*, 1990, **92**, 823; K. Q. Lao, E. Jensen, P. W. Kash and L. J. Butler, *J. Chem. Phys.*, 1990, **93**, 3958.
53 M. R. Wedlock and K. F. Freed, *J. Chem. Phys.*, 1991, **95**, 7275; R. A. Harris, M. R. Wedlock, L. J. Butler and K. F. Freed, to be published; M. R. Wedlock, E. Jensen, L. J. Butler and K. F. Freed, to be published.
54 R. Heather and H. Metiu, *J. Chem. Phys.*, 1989, **90**, 6903; S. Lee and K. F. Freed, *J. Chem. Phys.*, 1989, **90**, 7030; M. Jacon, O. Atabek and C. Leforestier, *J. Chem. Phys.*, 1989, **91**, 1585.
55 M. Berjot, M. Jacon and L. Bernard, *Opt. Commun.*, 1971, **4**, 117; 246.
56 A. H. Zewail, *J. Chem. Soc., Faraday Trans. 2*, 1989, **85**, 1221.
57 C. Wittig, personal communication; A. Garcia Vela, R. B. Gerber and J. J. Valentini, to be published.
58 M. I. McCarthy, R. B. Gerber and M. Shapiro, *J. Chem. Phys.*, 1990, **92**, 7708; U. Banin, A. Waldman and S. Ruhman, *J. Chem. Phys.*, 1992, **96**, 2416.

Paper 2/02294J; *Received* 23*rd March*, 1992